Abdelfatah *et al.*
Beni-Suef Univ J Basic Appl Sci (2022) 11:152
https://doi.org/10.1186/s43088-022-00331-y

Beni-Suef University Journal of Basic and Applied Sciences

RESEARCH

Open Access

Nonlinear analysis of Euler beams resting on a tensionless soil with arbitrary configurations

Heba Abdelfatah[1], Tamer Heshmat[2,3] and Mohamed Elshabrawy[2,3*]

Abstract

Background: The nonlinear interaction between an elastic Euler beam and a tensionless soil foundation is studied. The exact analytical solutions of the nonlinear problem are rather complicated. The main difficulty is imposing compatibility conditions at lift-off points. These points are determined as a part of the solution, although being needed to get the solution itself. In the current work, semi-analytical solutions are derived using the Rayleigh–Ritz method. The principle of vanishing variation of potential energy is adopted. The solution is approximated using a set of suitable trial functions. Accurate high-order approximate analytical solutions are obtained using MAXIMA symbolic manipulator. Lift-off points are identified through an iterative procedure and compatibility conditions are satisfied automatically. The methodology is designed to accommodate arbitrary configurations for the load distribution and the beam properties.

Results: Exact solutions are revised briefly to verify the semi-analytical solutions in terms of deflection, bending moment, and shear. Semi-analytical solutions for constant beam properties including various support conditions and load distributions are verified. Convergence of high-order semi-analytical solutions is illustrated for cases including one and two contact points. A parametric study is provided to illustrate the effect of soil stiffness on the contact length. The case of a finite beam with free ends is considered. The semi-analytical solutions for variable beam moment of inertia are provided and verified.

Conclusions: Highly accurate semi-analytical solutions can be obtained for the problem considered using the Rayleigh–Ritz method along with a symbolic manipulator. Arbitrary load and support configurations can be modeled, and the locations of lift-off points are well predicted. The semi-analytical solutions are extremely valuable for cases of variable moment inertia since exact solutions are rather rare.

Keywords: Rayleigh–Ritz, Maxima, Lift-off, Tensionless, Iterative procedure, Variable inertia, Free ends

1 Background

The soil–structure interaction engineering problems can be modeled as a beam or a plate resting on an elastic foundation. Practical examples of these are flexible column footings, mat foundations, strip foundations, railway structures [1], highway pavements, and pipelines [2, 3]. Flexible materials such as foam are used for cushioning in the furniture industries, automotive, and building soils all show highly nonlinear and viscoelastic behavior. It is required to model, predict, and understand both the dynamical and statistical behaviors of different structures which rest on these viscoelastic materials [4].

The viscoelastic supporting foundation can be modeled in different methods. Winkler is the simplest mathematical model for a continuously elastic foundation [5]. The Winkler model assumed that the base consists of closely

*Correspondence: mmshabrawy@nu.edu.eg

[2] Department of Engineering Mathematics and Physics, Faculty of Engineering, Cairo University, Giza, Egypt
Full list of author information is available at the end of the article

spaced, independent linear springs. Applied loads and the foundation's vertical deflection are parallel. The vertical displacements will be constantly under the loads whether the soil is subjected to a concentrated load or a uniformly distributed load. Also, the vertical deflection is zero outside the loading region for both loading cases [6]. Winkler has only one parameter. The Pasternak model assumed the presence of shear interactions between the linear springs [7] Shear interaction can be idealized by the connection of the springs' ends to a beam or plate composed of vertical incompressible elements which deflect only by lateral shear [8]. The Pasternak model has two parameters. The Pasternak model represents an extension of the Winkler model for elastic foundations.

Beams can be modeled as Euler–Bernoulli beams or Timoshenko beams. At low frequencies, both models give the same output results while at higher frequencies Timoshenko beam is more accurate[10, 11]. Many beam-foundation models, adopt an *ideal* Winkler or Pasternak assumptions, producing both tensile and compressive stresses in the soil due to beam–soil interaction [12]. In other words, the vertically downward displacement will cause compressive stresses in the foundation and the upward displacement will result in tensile stresses in the foundation. This methodology leads to non-physical results. Generally, the contact between the beam and its foundation is limited to regions of positive downward deflection. The negative upward deflection regions are contactless. The foundation has no resistance in contactless regions. In other words, the foundation tensile resistance at upward deflection is fictitious. Eliminating the fictitious tensile resistance is termed as a beam resting on tensionless soil (Fig. 1). This problem is complex because we need to determine the points of zero deflection, termed as the lift-off points [13]. Identifying the locations of lift-off points (Fig. 2) is necessary since they mark the boundaries of regions of contact [14, 15].

The present work will study the Euler–Bernoulli beam that rests on a tensionless Winkler foundation. Numerous analytical studies are available where infinite beams are considered. The infinite beam imposes problem symmetry [5]. Finite beam analysis is quite challenging because continuity conditions are necessary at lift-off focuses, [5] whose locations are unidentified a priori as shown in Fig. 2.

Numerical methods including the Boundary element method [16], finite element [17, 18], and the spline finite strip method [19] are efficient. However, the accuracy of numerical methods is influenced by a lot of parameters including the number of points,

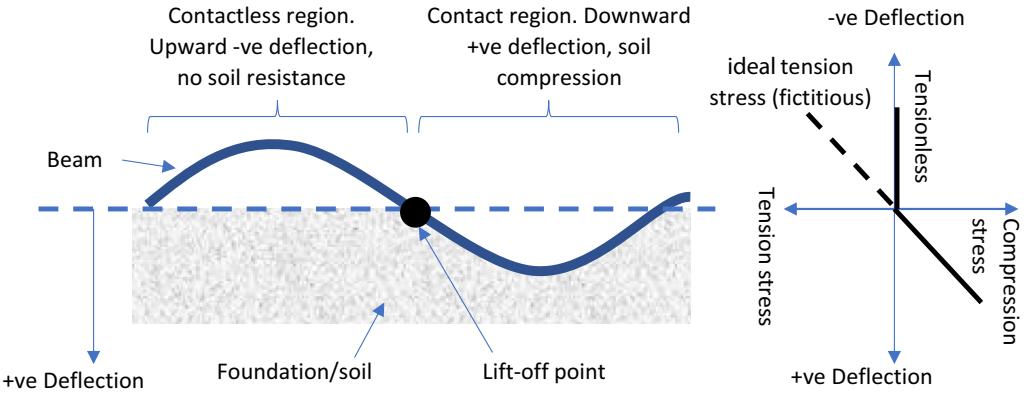

Fig. 1 Interaction of tensionless soil with a beam

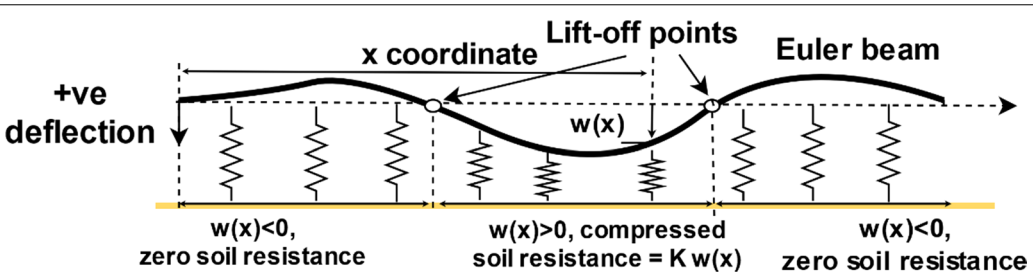

Fig. 2 A schematic of finite beam problem

discretization order, and the linear solver tolerance. Hence, solution verification, postprocessing, and regeneration are not always straightforward.

Fortunately, various powerful analytical methods have been developed in the past few years to analyze a wide spectrum of problems. For instance, the classical method of the Laplace transform was recently combined with the optimized composition method to solve the fractional nonlinear Boussinesq system [20] Another powerful technique is the method of Lie groups [21] that was applied recently to the two-dimensional Phi-Four equation [22]. Also, the method of reproducing kernel was applied to various nonlinear problems [23] and [24]. An alternative efficient method is the Rayleigh–Ritz method (RRM) [25]. The method represents a highly accurate semi-analytic series solution. Validated positions of lift-off points are obtained, avoiding the difficult method of imposing continuity. Results of the RRM are provided for various support and loading cases to introduce a parametric study for the different model parameters.

2 Methods

2.1 Governing equations

The beam equilibrium equation can be written as follows [3]:

$$\frac{d^2}{dx^{*2}}\left(EI^*\left(\frac{d^2w^*}{dx^{*2}}\right)\right)+K^*w^*-q^*=0 \tag{1}$$

where EI^* is the flexural stiffness of the beam; w^* is the vertical displacement of the beam; K^* is the Winkler foundation modulus; and q^* is the distributed load. Starred variables have dimensions of length (w^*, x^*), force per length (q^*), length power four (I^*), and force per length squared (K^*). It should be noted that I^* is generally a function of x^*. The standard procedure of normalization will be adopted. The quantities $\overline{q}$ and I are introduced, and they stand for reference load and inertia, respectively. They are assigned suitable reference values to guarantee that the dimensionless variables are close to one (neither too small nor too big). Dividing Eq. (2) by $\overline{q}$ the following is obtained:

$$\frac{d^2}{dx^{*2}}\left(\frac{EI^*\left(\frac{d^2w^*}{dx^{*2}}\right)}{\overline{q}}\right)+\frac{K^*w^*}{\overline{q}}-\frac{q^*}{\overline{q}}=0 \tag{2}$$

Define the dimensionless variables $x=x^*/L$, $w=w^*/\Delta$, $q=q^*/\overline{q}$, $i(x)=I^*/I$, $\Delta=L^4\overline{q}/(EI)$, $\overline{K}=K^*\Delta/\overline{q}$. Hence, the substitutions $x^*=Lx, w^*=w\Delta$, $q^*=q\overline{q}$, $I^*=Ii(x)$, $K^*=\overline{K}\overline{q}/\Delta$, $E=L^4\overline{q}/(I\Delta)$, are plugged into Eq. (2).

$$\frac{d^2}{L^2dx^2}\left(\frac{L^4\overline{q}}{I\Delta}\frac{\frac{Ii(x)\Delta}{L^2}\left(\frac{d^2w}{dx^2}\right)}{\overline{q}}\right)+\frac{\overline{K}\overline{q}}{\Delta}\frac{w\Delta}{\overline{q}}-\frac{q\overline{q}}{\overline{q}}=0 \tag{3}$$

The constant terms are factored out. Also, identical terms are canceled out from the denominator and numerator:

$$\frac{d^2}{dx^2}\left(i(x)\left(\frac{d^2w}{dx^2}\right)\right)+\overline{K}w-q=0 \tag{4}$$

Hence, the following equation is finally obtained:

$$\frac{d^2}{dx^2}\left(i(x)\left(\frac{d^2w}{dx^2}\right)\right)+Kw-q=0 \tag{5}$$

Referring to Fig. 3, the stiffness K of a tensionless soil is defined as:

$$K=\begin{cases}0w\le 0\\ \overline{K}w>0\end{cases} \tag{6}$$

Equation (6) can be rewritten using Heaviside step function U as follows:

$$K=\overline{K}U(w) \tag{7}$$

The normalized governing Eq. (5) is governed by three factors: $\overline{K}$, the load distribution q and $i(x)$. This property simplifies the analysis considerably. The dimensional bending moment M^* is equal to

$$M^*=EI^*\left(\frac{d^2w^*}{dx^{*2}}\right)=EI^*\frac{\Delta}{L^2}\left(\frac{d^2w}{dx^2}\right)=i(x)\overline{q}L^2\frac{d^2w}{dx^2} \tag{8}$$

Hence, the dimensionless bending moment M is defined as:

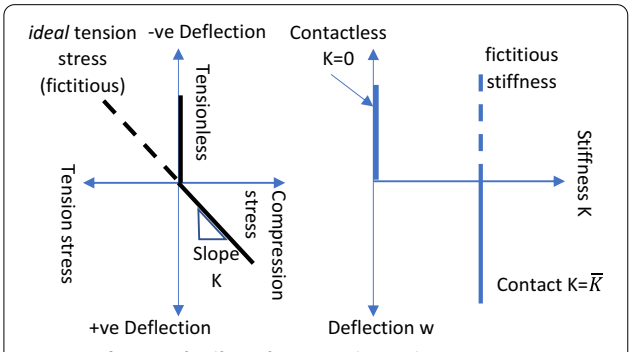

Fig. 3 Definition of stiffness for tensionless soil

$$M = \frac{M^*}{\overline{q}L^2} = i(x)\frac{d^2w}{dx^2} \tag{9}$$

Similarly, the dimensionless shear Q is defined and related to the dimensional shear Q^* as:

$$Q = \frac{Q^*}{\overline{q}L} = \frac{d}{dx}\left(i(x)\frac{d^2w}{dx^2}\right) \tag{10}$$

It should be noted that $x \in [0, 1]$.

2.2 Variational formulation

An equivalent form of Eq. (5) is obtained using standard procedures of calculus variations [5]:

$$\delta\phi = 0 \tag{11}$$

where δ is the variation operator and ϕ is the potential energy defined as:

$$\phi = \int_0^1 \left(\frac{i(x)}{2}\left(\frac{d^2w}{dx^2}\right)^2 + \frac{Kw^2}{2} - qw\right)dx \tag{12}$$

The variation of ϕ is equated to zero to find the equilibrium solution. The equivalence of Eq. (12) and Eq. (5) is explained briefly.

$$\delta\phi = 0 = \delta\int_0^1 \left(\frac{i(x)}{2}\left(\frac{d^2w}{dx^2}\right)^2 + \frac{Kw^2}{2} - qw\right)dx \tag{13}$$

Applying integration by parts twice to Eq. (13). The boundary terms arise as $i(x)\frac{d^2w}{dx^2}\frac{d\delta w}{dx}\Big|_0^1$ and $\frac{d}{dx}\left(i(x)\frac{d^2w}{dx^2}\right)\delta w\Big|_0^1$. Both terms vanish since $\frac{d}{dx}\left(\frac{d^2w}{dx^2}\right) = 0$,$\frac{d^2w}{dx^2} = 0$, and $\frac{dw}{dx} = 0$, for free, hinged, and clamped end conditions, respectively. The only remaining term is

$$\delta\phi = 0 = \int_0^1 \left(\frac{d^2}{dx^2}\left(i(x)\frac{d^2w}{dx^2}\right) + Kw - q\right)\delta w dx \tag{14}$$

Since δw is defined as an arbitrary quantity, the integrand is equated to zero. Hence, Eq. (5) is recovered.

2.3 Rayleigh–Ritz method

The solution w is approximated by $\widetilde{w}(x)$ defined as [5]:

$$\widetilde{w}(x) = \sum_{i=i_{\min}}^{N} a_i\widetilde{w}_i(x) \tag{15}$$

Here, $\widetilde{w}_i(x)$ is a set of trial functions. Generally, polynomials are chosen according to problem boundary conditions. The RRM solution is obtained by substitution of $w = \widetilde{w}_i(x)$ in Eq. (12). The resulting expression is

$$\delta\phi = 0 = \delta\int_0^1 \left(\frac{i(x)}{2}\left(\frac{d^2\sum_{i=i_{\min}}^{N} a_i\widetilde{w}_i(x)}{dx^2}\right)^2 + \frac{K\left(\sum_{i=i_{\min}}^{N} a_i\widetilde{w}_i(x)\right)^2}{2} - q\sum_{i=i_{\min}}^{N} a_i\widetilde{w}_i(x)\right)dx \tag{16}$$

The vanishing variation of the potential energy defined in Eq. (16) is imposed through:

$$\frac{\partial\phi}{\partial a_j} = 0 \tag{17}$$

Hence, Eq. (17) is used to rewrite Eq. (16) as follows:

$$\int_0^1 \left(i(x)\left(\frac{d^2\sum_{i=i_{\min}}^{N} a_i\widetilde{w}_i(x)}{dx^2}\right)\widetilde{w}_j(x) + K\left(\sum_{i=i_{\min}}^{N} a_i\widetilde{w}_i(x)\right)\widetilde{w}_j(x) - q\widetilde{w}_j(x)\right)dx = 0 \tag{18}$$

This can be written as a linear algebraic system of equations as follows:

$$\sum_{i=i_{\min}}^{N} A_{ji}a_i = B_j \tag{19}$$

The coefficient matrix A_{ji} and the right-hand side B_j are defined as:

$$A_{ji} = \int_0^1 \left(i(x)\left(\frac{d^2\widetilde{w}_i(x)}{dx^2}\right)\widetilde{w}_j(x) + K\widetilde{w}_i(x)\widetilde{w}_j(x)\right)dx \tag{20}$$

$$B_j = \int_0^1 q\widetilde{w}_j(x)dx \tag{21}$$

The algebraic linear system of equations is solved to obtain values of a_i. Hence, an analytical expression is obtained for $\widetilde{w}$. The whole procedure is implemented by the symbolic manipulator MAXIMA.

2.3.1 Tensionless Soil Problem Procedure

The main difficulty introduced by Eq. (6) is that w is not known a priori. Specifically, the points at which the sign of w changes should be determined to get the solution. These points are termed Lift-off points, and they are denoted by x_L and defined as:

$$w(x_L) = 0, x_L \in (0, 1) \tag{22}$$

The values of x_L are needed to calculate K using Eq. (6). Since $w \approx \widetilde{w}(x)$ is the output of the Rayleigh–Ritz method, an iterative is adopted to obtain x_L and the solution. An initial guess for x_L^n of $\widetilde{w}^n$ is used to get a further improved solution $\widetilde{w}^{n+1}$. The procedure is repeated till the convergence condition $x_L^n = x_L^{n+1}$ is satisfied. A flowchart illustrates the procedure in Fig. 2. The iterative Rayleigh–Ritz algorithm is listed:

1. Obtain the load distribution q. Initialize the iteration counter $n = 0$. Initialize x_L to any suitable value x_L^0. For simple loads use $x_L^0 = 1$, assuming full contact. Else, use $x_L^0 =$ roots of q, assuming that lift-off points will be close to zero load points.
2. Calculate $K = K(x)$ based on Eq. (6) using x_L^n.
3. Obtain the coefficient matrix A_{ji} and right-hand side vector B_j, using Eqs. (20) and (21). Hence, solve Eq. (19) and calculate a_i.
4. Find an approximate expression for the $w \approx \widetilde{w}^n(x)$ using Eq. (15). Hence, solve Eq. (22) and obtain x_L^{n+1}.
5. Check the convergence condition $x_L^n \stackrel{?}{=} x_L^{n+1}$. If yes, then end calculations and use $\widetilde{w}^n$ as the final solution. Else, update $x_L^n = x_L^{n+1}$, and $n = n + 1$, and go to step 2.

The characteristics of the iterative procedure are given as follows:

- The main input to the algorithm is the load distribution q. Also, variable inertial can be modeled using $i(x)$.
- The single convergence criterion is reaching a converged value of the lift-off points location.
- The converged value of x_L is typically reached within 10 iterations. More details will be provided in the discussion section.
- As more expansion terms are included in Eq. (15), the converged value of x_L should approach the exact value. Hence, the accuracy should generally improve as N increases.
- The main output of the algorithm is the RRM deflection $\widetilde{w}(x)$ calculated using the coefficients a_i. Once the deflection is determined, the bending moments and shear forces are calculated by differentiation.

2.4 General exact solution

Generally, deriving the exact solution is tedious. Still, the exact solution will be presented for various cases to verify the results of the Rayleigh–Ritz method. Hence, the exact solution methodology will be provided for a concise presentation.

Consider a piecewise fourth-order polynomial load $q(x) = Ax^4 + Bx^3 + Cx^2 + Dx + E$. The exact solution of Eq. (5) is only available in the case of $i(x) =$ constant. In this case, Eq. (5) is turned to

$$\frac{d^4w}{dx^4} + Kw - q = 0 \tag{23}$$

The exact solution of Eq. (23) is the sum of the homogeneous and the particular solutions, denoted by w_H and w_P, respectively.

$$w_H = \begin{cases} w_{H1} = \frac{A}{1680}x^8 + \frac{B}{840}x^7 + \frac{C}{360}x^6 + \frac{D}{120}x^5 \\ \quad + \frac{E}{24}x^4 + Fx^3 + Gx^2 + Hx + I \\ w_{H2} = (C_1\cos(\beta x) + C_2\sin(\beta x))\exp(-\beta x) \\ \quad + (C_3\cos(\beta x) + C_4\sin(\beta x))\exp(\beta x) \end{cases} \begin{matrix} , K = 0 \\ , K = \overline{K} \neq 0, \beta = \frac{\overline{K}^{\frac{1}{4}}}{\sqrt{2}} \end{matrix} \tag{24}$$

$$w_P = \frac{A}{\overline{K}}x^4 + \frac{B}{\overline{K}}x^3 + \frac{C}{\overline{K}}x^2 + \frac{D}{\overline{K}}x + \frac{E}{\overline{K}} - \frac{24A}{\overline{K}^2} \quad K = \overline{K} \neq 0, q \neq 0 \tag{25}$$

Here, the symbols $F, G, H, I, C_1, C_2, C_3$, and C_4 are integration constants. For each specific case, boundary and compatibility conditions are used to find the correct combination of w_H and w_P that describes the problem.

The boundary conditions differ depending on the considered geometry. Two support conditions are considered. The clamped–clamped beam is considered as defined by the following boundary conditions:

$$w(x = 0) = w(x = 1) = \frac{dw(x = 0)}{dx} = \frac{dw(x = 1)}{dx} = 0 \tag{26}$$

In addition, the free-free beam is considered with the following boundary conditions:

$$\frac{d^2w(x = 0)}{dx^2} = \frac{d^2w(x = 1)}{dx^2} = \frac{d^3w(x = 0)}{dx^3} = \frac{d^3w(x = 1)}{dx^3} = 0 \tag{27}$$

The reader is reminded that q and K are defined using piecewise expressions. This is attributed to the load nature in the case of q, and the variable soil-beam contact in the case of K. Compatibility conditions need to be satisfied at the boundary points of each piece. Generally, boundary points occur at lift-off points and abrupt changes of q. The compatibility conditions that need to be satisfied at a boundary point are:

$$w(x = x_b^-) = w(x = x_b^+) \tag{28}$$

$$\frac{dw(x=x_b^-)}{dx} = \frac{dw(x=x_b^+)}{dx} \tag{29}$$

$$\frac{d^2w(x=x_b^-)}{dx^2} = \frac{d^2w(x=x_b^+)}{dx^2} \tag{30}$$

$$\frac{d^3w(x=x_b^-)}{dx^3} = \frac{d^3w(x=x_b^+)}{dx^3} \tag{31}$$

Here, $w(x=x_b^-)$ and $w(x=x_b^+)$ stand for the one-sided limits $\lim_{x\to x_b^-} w(x)$, and $\lim_{x\to x_b^+} w(x)$, respectively. The geometric boundary conditions require continuity of the displacement and slope [2] which are satisfied in Eq. (28) and (29). Also, the natural boundary conditions require the continuity of bending moment and shear force [2] which are satisfied in Eq. (30) and (31).

Based on the nature of the load of each case along with boundary conditions, the number of boundary points is determined. Therefore, the compatibility conditions of the system are identified to obtain the integration constants. The steps for deriving the exact solution are listed:

1. Obtain the load distribution q. Based on this distribution, the full beam domain $x \in [0, 1]$ is divided into separate regions. Each region is identified based on expected beam–soil contact and the expression of q. For instance, regions with expected upwards deflection are assigned $K = 0$.
2. For each region, determine the correct combination of homogeneous and particular solutions, using Eqs. (24) and (25). For each region, a set of 4 integration constants should be defined.
3. Define the system of equations used to calculate the integration constants. This system is based on applying the following boundary conditions:
   a. Beam support boundary conditions are provided by Eq. (26) for clamped–clamped beams or Eq. (27) for free-free beams.
   b. Compatibility conditions imposed at the boundaries of regions as listed in Eqs. (28)–(31).
4. The algebraic system obtained in step 3 includes dozens of linear equations. In addition, it includes the locations of lift-off points. Hence, this system is generally nonlinear and should be solved using a suitable iterative scheme in MAXIMA.

The application of these steps will be further clarified for each case.

3 Discussion

Five different cases are presented to show the accuracy of the current method. The cases include various loading profiles and boundary conditions. In addition to considering beam with constant inertia, where $i(x) =$ constant, and beam with variable inertia, where $i(x) = f(x)$. The solutions may include one or more lift-off points and symmetric and non-symmetric behavior. Table 1 shows the formulas describing loading conditions q, number of

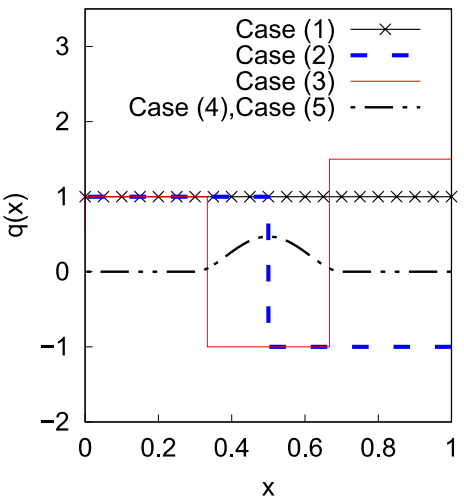

Fig. 4 Investigated loads profiles q

Table 1 Various loading q, soil stiffness, and support conditions for the five cases

Case	Load q	Number of lift-off points	$\overline{K}$	Support condition
1	$U(x)$	0	500	Clamped–clamped
2	$U(x) - 2U\left(x - \frac{1}{2}\right)$	1	500	Clamped–clamped
3	$U(x) - 2U\left(x - \frac{1}{3}\right) + 2.5U\left(x - \frac{2}{3}\right)$	2	500	Clamped–clamped
4, 5	$\left(U\left(x - \frac{3}{10}\right) - U\left(x - \frac{7}{10}\right)\right) \times \left(\frac{9375x^4}{32} - \frac{9375x^3}{16} + \frac{26625x2}{64} - \frac{7875x}{64} + \frac{6615}{512}\right)$ $+ \frac{26625x2}{64} - \frac{7875x}{64} + \frac{6615}{512}\Big)$	2	1250	Free-free

lift-off point, the soil stiffness $\overline{K}$, and the support condition for each case. Also, the load functions q are plotted in Fig. 4.

The exact solution and RRM analytical solution are presented for the first four cases which deal with uniform beams under the effect of different loading conditions. For symmetric cases, RRM solutions are provided for even values of N. The RRM deflection $\widetilde{w}(x)$ approaches the exact solution w as N increases. The convergence is further illustrated by the plotting of percentage error for the first four different cases. The convergence of RRM shear and moment toward the exact values are illustrated and proved through different comparison figures. Only RRM solutions are presented for the fifth case of variable inertia since there is no exact solution for such a case. The accuracy of the RRM solutions is proved through comparison with high values of N.

3.1 Case (1)

Generally, four boundary conditions are required to solve Eq. (5). For the specific case of a clamped–clamped beam, the boundary conditions are in Eq. (26).

Consider the load $q = q_1$ defined as:

$$q_1 = 1 \tag{32}$$

The case is rather simple since it does not include any contact points. However, it is included to illustrate the basic features of the exact and RRM solutions.

3.1.1 Exact solution

The exact solution, in this case, is given by:

$$w = w_{H2} + w_p \tag{33}$$

$$w_p = \frac{q_1}{\overline{K}} \tag{34}$$

Using an arbitrary value of $\overline{K} = 500$. The exact solution is:

$$w = (-0.002087187\cos(\beta x) - 0.002115979\sin(\beta x))\exp(-\beta x) + 1/500 \\ +(8.718666982 \times 10^{-5}\cos(\beta x) - 5.839393538 \times 10^{-5}\sin(\beta x))\exp(\beta x), \ \beta = \overline{K}^{0.25}/\sqrt{2} \tag{35}$$

3.1.2 RRM solution

The following set of trial functions is selected based on the boundary conditions of Eq. (26)

$$\widetilde{w}_i(x) = (1-x)^2 x^i \tag{36}$$

Here, $i_{\min} = 2$. This set of shape functions satisfies the conditions in Eq. (26). The set is illustrated in Fig. 5 for $\widetilde{w}_2(x)$, $\widetilde{w}_3(x)$ and $\widetilde{w}_4(x)$.

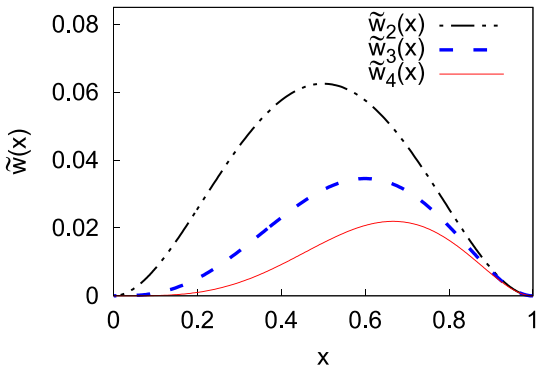

Fig. 5 Mode shapes for clamped–clamped beam

The exact solution is shown along with the RRM analytical solution in Fig. 6. Due to the symmetric nature of the problem, RRM solutions are provided for the two even values N=2,4. The RRM deflection $\widetilde{w}_i(x)$ approaches the exact solution w as N increases. This is clarified in Fig. 6A. The coefficients of RRM solutions are provided in Table 2.

The percentage error is defined as

$$100 \times (w - \widetilde{w})/|w_{\max}| \tag{37}$$

For case 1, $w_{\max} = w(x = 0.5) = 0.001288004$. The convergence is further illustrated in Fig. 6B, where the percentage error is plotted. The maximum error value for $N = 2$ is less than 1.5%, while for $N = 4$ the error is almost negligible. The convergence of RRM shear and moment toward the exact values is illustrated in Fig. 6C and D, respectively.

3.2 Case (2)

Consider the load $q = q_2$ defined as:

$$q_2 = U(x) - 2U\left(x - \frac{1}{2}\right) \tag{38}$$

3.2.1 Exact solution

This case includes one lift-off point. Hence, it is more complex compared to case 1. For this case, the solution is divided into three regions. Region 1 is defined as $x \in [0, x_1]$, where x_1 is equal to the contact length. Region 1 corresponds to downward deflection and downward load. Region 2 corresponds to upward deflection and downward load. Finally, region 3 corresponds to upward deflections and upward load. Hence,

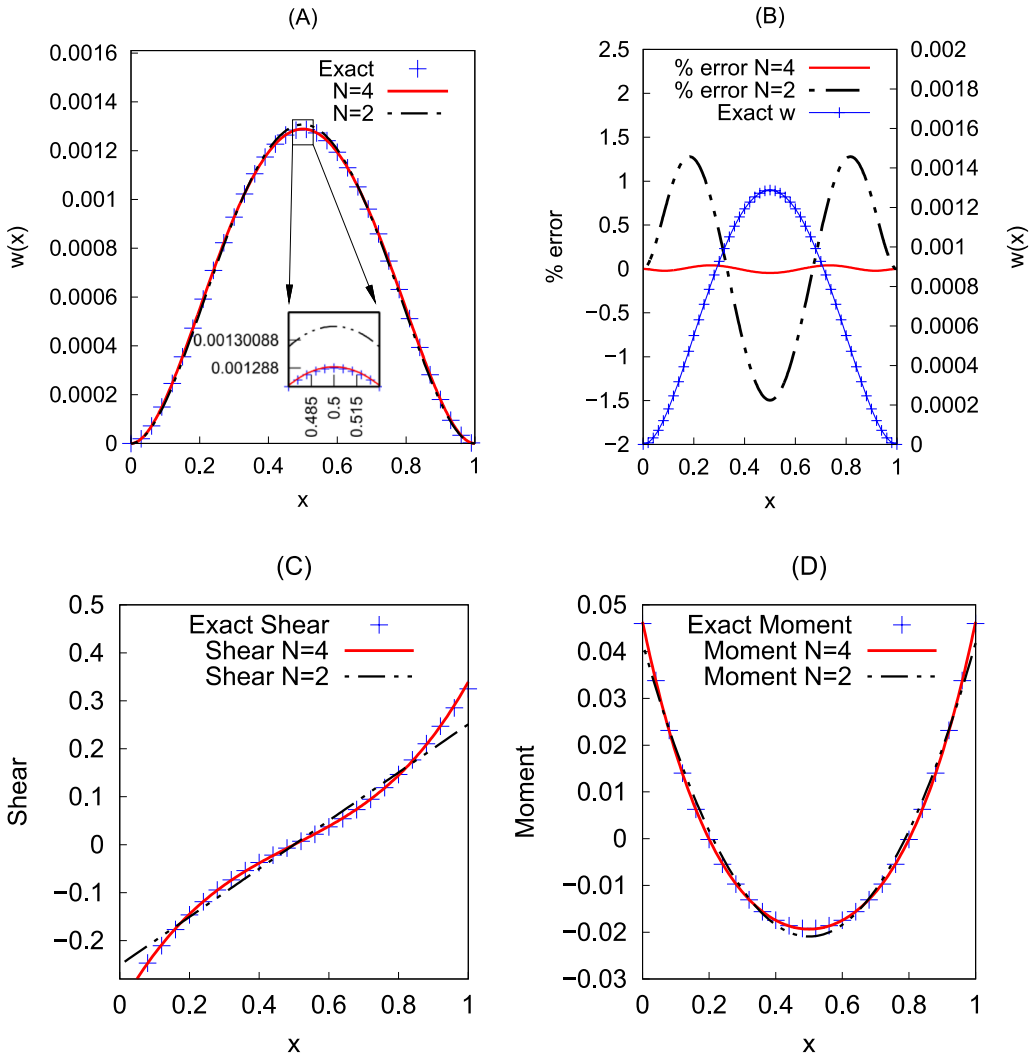

Fig. 6 Case (1) RRM and exact results. **A** Exact solution and RRM solutions. **B** Exact deflection and percentage error for various orders. **C** Exact and RRM shear. **D** Exact and RRM moment

Table 2 Coefficients a_i for various N of Rayleigh–Ritz procedure in case (1)

Coefficients a_i	$N = 4$	$N = 2$
a_2	$1.021450946 \times 10^{-2}$	$2.091633466 \times 10^{-2}$
a_3	$-1.021450946 \times 10^{-2}$	–
a_4	$2.317122185 \times 10^{-2}$	–

the following conditions should be satisfied based on the problem physics:

$$w = \begin{cases} w|_{q_2=+1,K=\overline{K}} = w_{H2} + w_p, 0 < x < x_1 \\ w|_{q_2=+1,K=0} = w_{H1}, x_1 \le x \le 0.5 \\ w|_{q_2=-1,K=0} = w_{H1}, 0.5 \le x \le 1 \end{cases} \tag{39}$$

$$w_p = \frac{1}{K} \tag{40}$$

$$w|_{q_2=+1,K=\overline{K}}(x = x_1) = 0 \tag{41}$$

The three functions $w|_{q_2=+1,K=\overline{K}}$, $w|_{q_2}=+1, K=0$, $w|_{q_2}=-1, K=0$, defined in Eq. (39) include 12 integration constants. In addition to the lift-off point x_1, hence there are total of 13 unknowns. Thus, a system of 13 algebraic equations should be solved to obtain the integration constants and x_1. The compatibility conditions, Eqs. (28) to (31), should be satisfied at the continuity points $x = 0.5$ and $x = x_1$, thus there are 8 compatibility conditions. Along with the four

Table 3 Integration constants for exact solutions of case (2)

	(1) $x \in [0, 0.461677498]$	(2) $x \in [0.461677498, 1/2]$	(3) $x \in [1/2, 1]$
C_1	−0.001950228	0	0
C_2	−0.001547479	0	0
C_3	$-4.977211027 \times 10^{-5}$	0	0
C_4	$-3.529768133 \times 10^{-4}$	0	0
A	0	0	0
B	0	0	0
C	0	0	0
D	0	0	0
E	1	1	−1
F	0	−0.053117020	0.113549646
G	0	0.017830983	−0.107169017
H	0	−0.001310906	0.040355761
I	0	$1.386093559 \times 10^{-4}$	−0.005069724

boundary conditions in Eq. (26), therefore there are total of twelve equations.

The solution is obtained by guessing $x_1 = 1/2$ and solving the resulting linear system Eq. (26) and Eqs. (28) to (31). The guessed value of x_1 is checked to satisfy Eq. (41) about $x_1 = 1/2$. The whole procedure can be implemented within any standard numerical root finding procedure.

An arbitrary value of $\overline{K} = 500$ is used. The exact contact length is obtained as $x_1 = 0.461677498$. The exact solution w is defined in terms of the integration constants provided in Table 3.

3.2.2 RRM solution

The Rayleigh–Ritz procedure is applied to clarify its success. Results are obtained for various $N = 5, 6, 7$. The initial guess of $x_1 = 1$ is adopted for different N. Convergence of x_1 is provided in Table 4. For all cases, convergence is achieved in six iterations. The converged value of x_1 for values of N is provided in Table 5. As expected, the highest N=7 yields $x_1 = 0.461079117$ in which the closest to the exact value $x_1 = 0.461677498$. The coefficients

Table 4 Rayleigh–Ritz convergence of contact length x_1 at $q = q_1$ for various N

Iteration number	$x_1 (N = 7)$	$x_1 (N = 6)$	$x_1 (N = 5)$
0 (initial guess)	1.0	1.0	1.0
1	0.5	0.5	0.5
2	0.462398107	0.461777190	0.461552264
3	0.461080697	0.460416937	0.460193392
4	0.461079117	0.460415253	0.460191732
5	0.461079117	0.460415253	0.460191732
6 (convergence)	0.461079117	0.460415253	0.460191732

Table 5 Contact length x_1 at $q = q_1$ for various N The exact value $x_1 = 0.461677498$

N	x_1
3	0.457752498
4	0.458442182
5	0.460191732
6	0.460415253
7	0.461079117

of RRM solutions are provided in Table 6. The percentage error is defined by Eq. (37).

For case 3. $|w_{\max}| = 3.902884943334274 \times 10^{-4}$ at $x = 0.6959982854779297$. The exact solution is shown along with the RRM analytical solution in Fig. 7A. The error is plotted in Fig. 7B for various N. The exact w is also plotted and a secondary y axis is used to accommodate scale difference. The error is minimum at the highest $N = 7$ with maximum $\approx 0.5\%$. The convergence of RRM shear and moment toward the exact values is illustrated in Fig. 7C and D, respectively.

3.2.3 Parametric study

To examine the influence of different $\overline{K}$ values on the lift-off point x_1, a parametric study is conducted. In Fig. 8, the variation of x_1 with $\overline{K}$ is plotted. The results of the exact and RRM method are provided. As the value of $\overline{K}$ gets higher, the soil stiffness increases, and the value of the lift-off point, x_1, decreases and gets closer to the beam's first edge. Hence, increasing soil stiffness decreases the contact length. This is expected since stronger soil would carry the load at a smaller length. Another important observation is how RRM is close to the exact solution for the wide range of $\overline{K}$ considered.

3.3 Case (3)

Consider the load $q = q_3$ defined as:

$$q_3 = U(x) - 2U\left(x - \frac{1}{3}\right) + 2.5U\left(x - \frac{2}{3}\right) \tag{42}$$

This case includes two lift-off points. Hence, it is more complex than case 2 and sheds more light on the power of RRM.

3.3.1 Exact solution

The load is not symmetric and deriving an exact solution is more difficult compared to case 2. In the current case, the beam contacts the ground at $x \in [0, x_1] \cup [x_2, 1]$ and has an upward deflection region for $x \in]x_1, x_2[$. Hence, the following regions are defined:

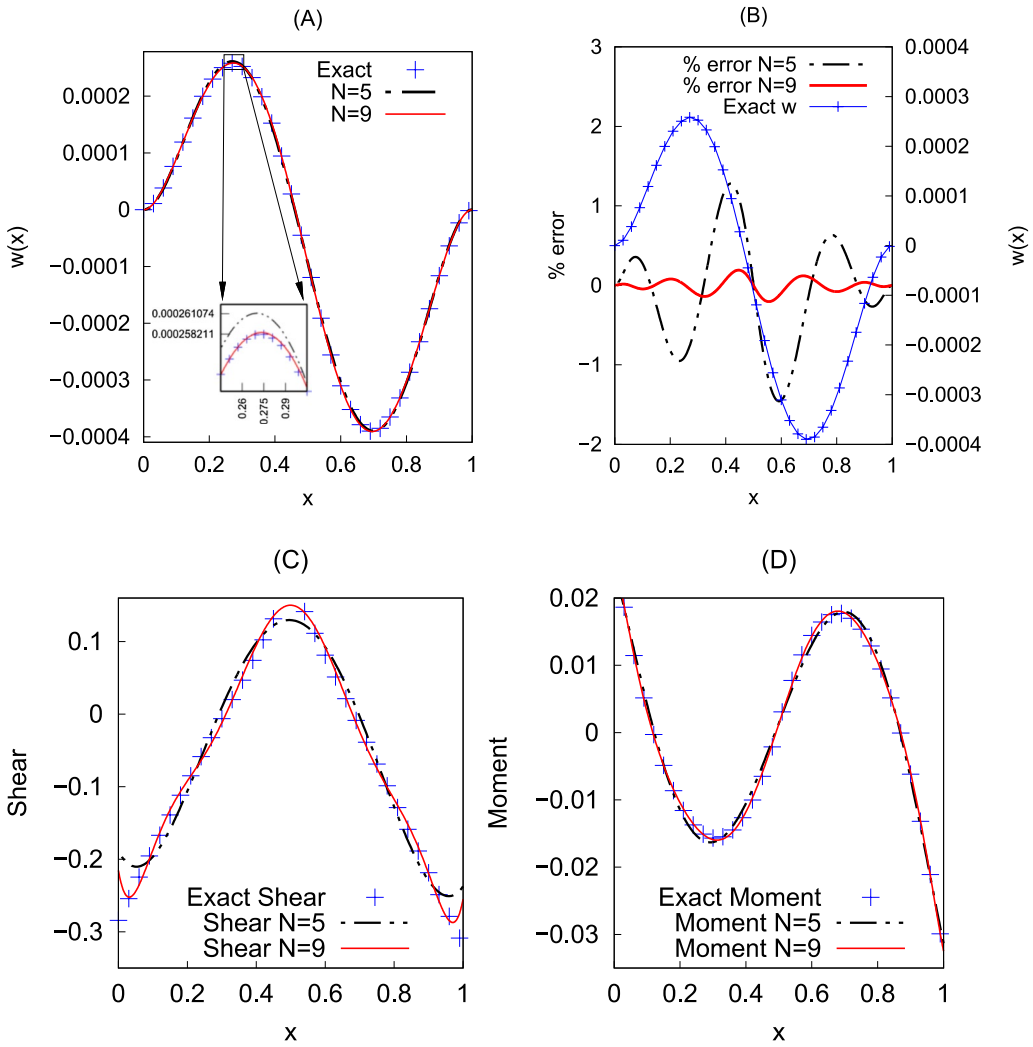

Fig. 7 Case (2) RRM and exact results. **A** Exact solution and RRM deflection. **B** Exact deflection and percentage error for various orders. **C** Exact and RRM shear. **D** Exact and RRM moment

Table 6 Coefficients a_i for various N of Rayleigh–Ritz procedure in case (2)

Coefficients a_i	$N = 7$	$N = 6$	$N = 5$
a_2	$1.389441157 \times 10^{-2}$	$1.243649123 \times 10^{-2}$	$1.228951157 \times 10^{-2}$
a_3	$-3.304185325 \times 10^{-2}$	$-8.681772789 \times 10^{-3}$	$-6.93056228 \times 10^{-3}$
a_4	$7.872285806 \times 10^{-2}$	$-5.513087168 \times 10^{-2}$	$-6.169062329 \times 10^{-2}$
a_5	$-2.901323256 \times 10^{-1}$	$3.105833821 \times 10^{-2}$	$4.067911857 \times 10^{-2}$
a_6	$3.527987667 \times 10^{-1}$	$4.811333937 \times 10^{-3}$	–
a_7	$-1.392163461 \times 10^{-1}$	–	–

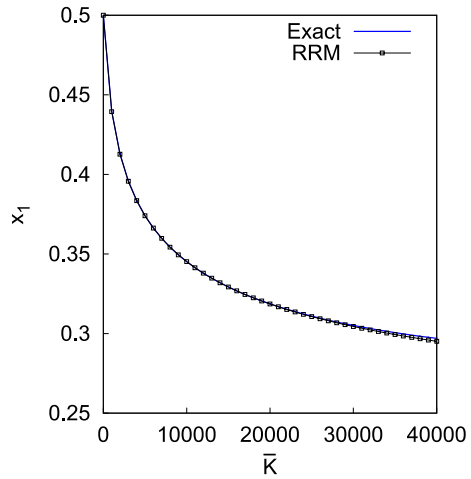

Fig. 8 Case (2) Variation of lift-off point, x_1, for different values of $\overline{K}$

$$w = \begin{cases} w|_{q_3=+1,K=\overline{K}} = w_{H2} + w_p, & 0 < x < x_1 \\ w|_{q_3=+1,K=0} = w_{H1}, & x_1 \le x \le \frac{1}{3} \\ w|_{q_3=-1,K=0} = w_{H1}, & \frac{1}{3} \le x \le \frac{2}{3} \\ w|_{q_3=+1.5,K=0} = w_{H1}, & \frac{2}{3} \le x \le x_2 \\ w|_{q_3=+1.5,K=\overline{K}} = w_{H2} + w_p, & x_2 \le x \le 1 \end{cases} \tag{43}$$

$$w|_{q_3=+1,K=\overline{K}}(x = x_1) = 0 \tag{44}$$

$$w|_{q_3=+1.5,K=0}(x = x_2) = 0 \tag{45}$$

The five functions defined in Eq. (43) include 20 integration constants; in addition to x_1 and x_2 ,hence there are total of 22 unknowns. Therefore, 22 algebraic equations are required to solve the system. Along with the 4 boundary conditions in Eq. (26), the compatibility conditions, Eqs. (28) to (31), should be satisfied at the 4 continuity points: $x = x_1, x = 1/3, x = 2/3$, and $x = x_2$, thus there are 16 compatibility conditions and total of 20 equations.

A similar procedure to case (2) is followed to solve the system of equations. The solution starts by guessing $x_1 \approx 0.2$ and $x_2 \approx 0.7$, then solving the linear system of Eqs. (26) to (31). Next check the guessed values of x_1 and x_2 by finding roots of Eq. (44) and Eq. (45) about the guessed x_1 and x_2. Using arbitrary value of $\overline{K} = 500$, the lift-off points are determined as $x_1 = 0.160090758$ and $x_2 = 0.720646326$. The exact solution w is defined in terms of the integration constants provided in Table 7.

3.3.2 RRM solution

For the current case, the initial guess of $x_1 = 1/3$ and $x_2 = 2/3$. The converged values of x_1 and x_2 for different N are provided in Table 8. For all N values, convergence is achieved in four iterations. The coefficients of RRM solutions are provided in Table 9. The exact solution is shown along with the RRM analytical solution in Fig. 9A for $N = 5$ and 9. Using the exact solution, $\max|w| = 3.027998651 \times 10^{-4}$ at $x = 0.473493180$. The percentage error in deflection of $N = 5$ compared to exact solution is less than or equal 5.6%, while for $N = 9$ the percentage error in deflection shown in Fig. 9A, B is negligible. The convergence of RRM shear and moment toward the exact values is illustrated in Fig. 9C and D, respectively.

Table 7 Integration constants for exact solutions of cases (3)

	***Region*(1)** $x \in [0, 0.160090758]$	***Region*(2)** $x \in [0.160090758, \frac{1}{3}]$	***Region*(3)** $x \in [\frac{1}{3}, \frac{2}{3}]$	***Region*(4)** $x \in [\frac{2}{3}, 0.720646326]$	***Region*(5)** $x \in [0.720646326, 1]$
C_1	−0.001605594	0	0	0	0.016128141
C_2	$-7.740305847 \times 10^{-4}$	0	0	0	−0.014338152
C_3	$-3.944056866 \times 10^{-4}$	0	0	0	$9.845320141 \times 10^{-5}$
C_4	$4.371580421 \times 10^{-4}$	0	0	0	$3.306944455 \times 10^{-5}$
A	0	0	0	0	0
B	0	0	0	0	0
C	0	0	0	0	0
D	0	0	0	0	0
E	1	1	−1	1.5	1.5
F	0	−0.030274937	0.080836174	−0.196941604	0
G	0	0.003791446	−0.051764109	0.226013669	0
H	0	$-2.634142922 \times 10^{-6}$	0.012343045	−0.111113745	0
I	0	$9.913674928 \times 10^{-8}$	−0.001028707	0.019547424	0

Table 8 Lift-off points x_1 and x_2 at $q = q_3$ for various N The exact value $x_1 = 0.160090758$ and $x_2 = 0.720646326$

N	x_1	x_2
3	–	0.861781925
4	0.160526961	0.731332093
5	0.160613269	0.731275350
6	0.163320452	0.722140163
7	0.162688881	0.722102016
8	0.160298079	0.721228451
9	0.160497934	0.721098214

3.3.3 Parametric study

In this case, the parametric study examines the effect of different $\overline{K}$ values on the two lift-off points x_1 and x_2 for both exact solution and RRM. The variation against $\overline{K}$ is shown in Fig. 10A and B for x_1 and x_2, respectively. As $\overline{K}$ increases, the value of the first lift-off point, x_1, decreases and gets closer to the first beam edge as shown in Fig. 10A, while the value of the second lift-off point, x_2, increases and gets closer to the second beam edge as shown in Fig. 10B. Hence, the contact length decreases as a result of increasing the soil stiffness. Furthermore, for this case of two lift-off points, RRM accuracy is illustrated by comparison with the exact solution. The convergence of RRM shear and moment toward the exact values is illustrated in Fig. 10C and D, respectively.

3.4 Case (4)

For a beam with free ends, zero shear and bending moment are assumed at the far left and right edges. Hence, the beam boundary conditions are defined by Eq. (27).

Consider the load $q = q_4$ defined as:

$$q_4 = \left(u\left(x-\frac{3}{10}\right) - u\left(x-\frac{7}{10}\right)\right)\left(\frac{9375x^4}{32} - \frac{9375x^3}{16} + \frac{26625x^2}{64} - \frac{7875x}{64} + \frac{6615}{512}\right) \tag{46}$$

3.4.1 Exact solution

In this case, the beam contacts the ground at $x \in [x_1, x_2]$. Therefore, the following conditions should be satisfied:

$$w = \begin{cases} w|_{q_4=0,K=0} = w_{H1}, & 0 < x < x_1 \\ w|_{q_4=0,K=\overline{K}} = w_{H2}, & x_1 \le x \le 0.3 \\ w|_{q_4=f(x),K=\overline{K}} = w_{H2} + w_p, & 0.3 \le x \le 0.7 \\ w|_{q_4=0,K=\overline{K}} = w_{H2}, & 0.7 \le x \le x_2 \\ w|_{q_4=0,K=0} = w_{H1}, & x_2 \le x \le 1 \end{cases} \tag{47}$$

$$w|_{q_4=0,K=0}(x = x_1) = 0 \tag{48}$$

$$w|_{q_4=0,K=0}(x = x_2) = 0 \tag{49}$$

The five functions defined in Eq. (47) include 20 integration constants, in addition to x_1 and x_2 hence there are total of 22 unknowns. Along with the 4 boundary conditions in Eq. (27), the compatibility conditions, Eqs. (19) to (22), should be satisfied at the 4 continuity points: $x = x_1, x = 0.3, x = 0.7$, and $x = x_2$, thus there are 16 compatibility conditions and total of 20 equations.

Similarly to the previous cases, the solution starts by guessing $x_1 \approx 0.2$ and $x_2 \approx 0.8$, then solving the linear system of Eqs. (26) to (31). Next check the guessed values of x_1 and x_2 by finding roots of Eq. (48) and Eq. (49) about the guessed x_1 and x_2. Using arbitrary value of $\overline{K} = 1250$, the lift-off points are determined as $x_1 = 0.104030928$ and $x_2 = 0.895969072$. The exact solution w is defined in terms of the integration constants provided in Table 10.

Table 9 Coefficients a_i for various N of Rayleigh–Ritz procedure in case (3)

Coefficients a_i	$N = 9$	$N = 7$	$N = 5$
a_2	$3.693980624 \times 10^{-3}$	$2.982531822 \times 10^{-3}$	$6.741008214 \times 10^{-3}$
a_3	$-2.171660765 \times 10^{-2}$	$-7.087635317 \times 10^{-3}$	$-5.122002053 \times 10^{-2}$
a_4	$-3.000365755 \times 10^{-3}$	$-1.021538762 \times 10^{-1}$	$5.763218439 \times 10^{-2}$
a_5	$-7.178569399 \times 10^{-2}$	$2.170854003 \times 10^{-1}$	$-2.676483347 \times 10^{-4}$
a_6	$2.623333605 \times 10^{-1}$	$-8.320853304 \times 10^{-2}$	–
a_7	$-4.084992482 \times 10^{-2}$	$-1.891235161 \times 10^{-2}$	–
a_8	$-2.669188602 \times 10^{-1}$	–	–
a_9	$1.479964372 \times 10^{-1}$	–	–

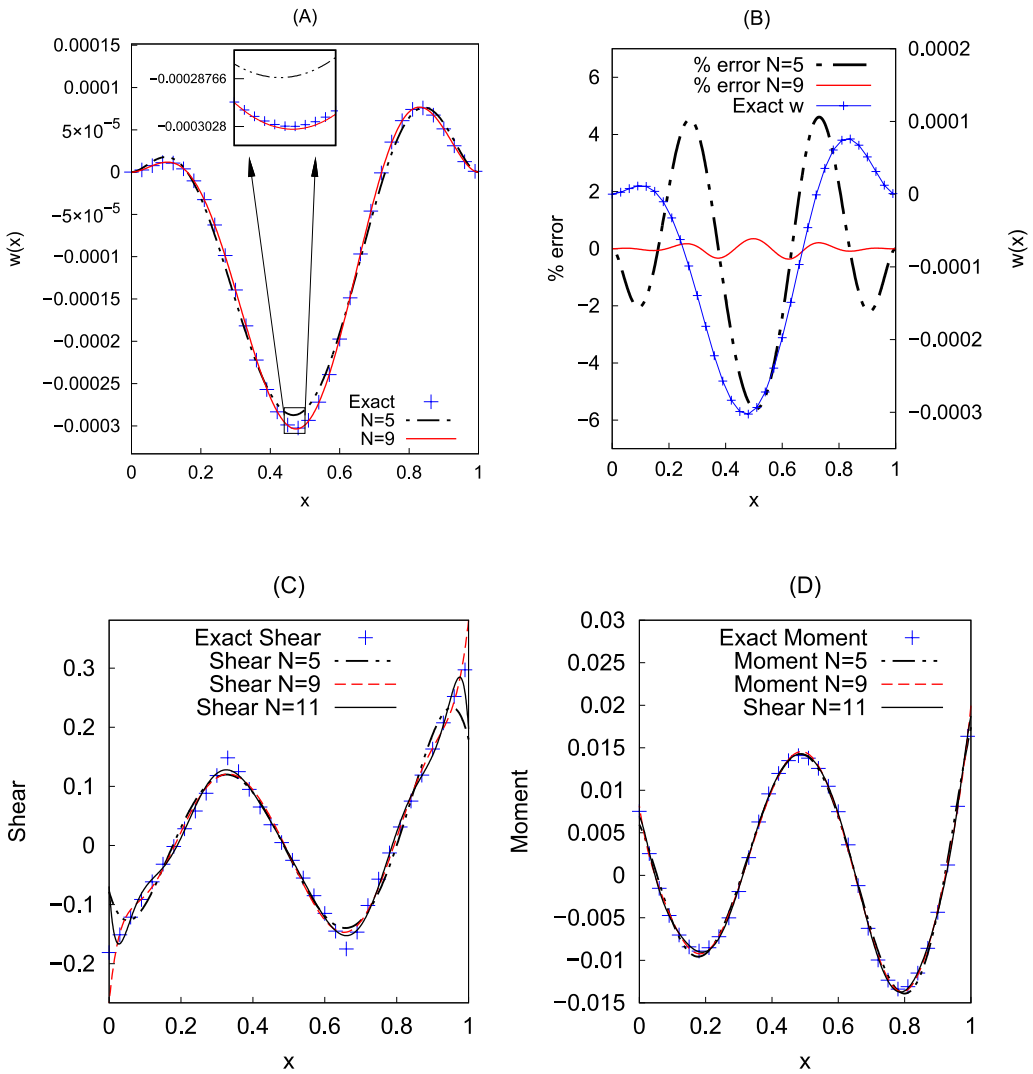

Fig. 9 Case (3) RRM and exact results. **A** Exact solution and RRM deflection. **B** Exact deflection and percentage error for various orders. **C** Exact and RRM shear. **D** Exact and RRM moment

3.4.2 RRM solution

The set of shape functions for free ends case is $\widetilde{w}_i(x) = T_i(x)$ are shown in Fig. 11. Here, $T_i(x)$ is the standard Chebyshev polynomials of the first kind of order i. The shape function is expressed as [26]:

$$T_i(x) = \cos\left(i \times \cos^{-1}(x)\right) \tag{50}$$

The value of $i_{\min} = 0$. However, the selected shape function does not satisfy the boundary conditions. Therefore, we need to impose the boundary conditions using additional 4 equations, Eq. (27). Thus, an overdetermined system of equations, where there are more questions than unknowns, needs to be solved to get the values of a_i. For example, in case of $N = 15$ there are 19 equations with 15 unknowns, Eq. (17). The least squares method is used to solve the overdetermined system of equations.

Starting with an initial guess of $x_1 = 0.1$ and $x_2 = 0.9$. The converged values of x_1 and x_2 for different N are provided in Table 11. For all N values, convergence is achieved in four iterations.

Using the exact solution, $\max|w| = 1.693292233 \times 10^{-4}$ at $x = 0.4999537766$. The exact solution is shown along with the RRM solution in Fig. 12A for $N = 7, 11$ and 15 in Fig. 12A and B. The coefficients of RRM solutions are provided in Table 11. The convergence of RRM shear and moment toward the exact values is illustrated in Fig. 7C and D, respectively.

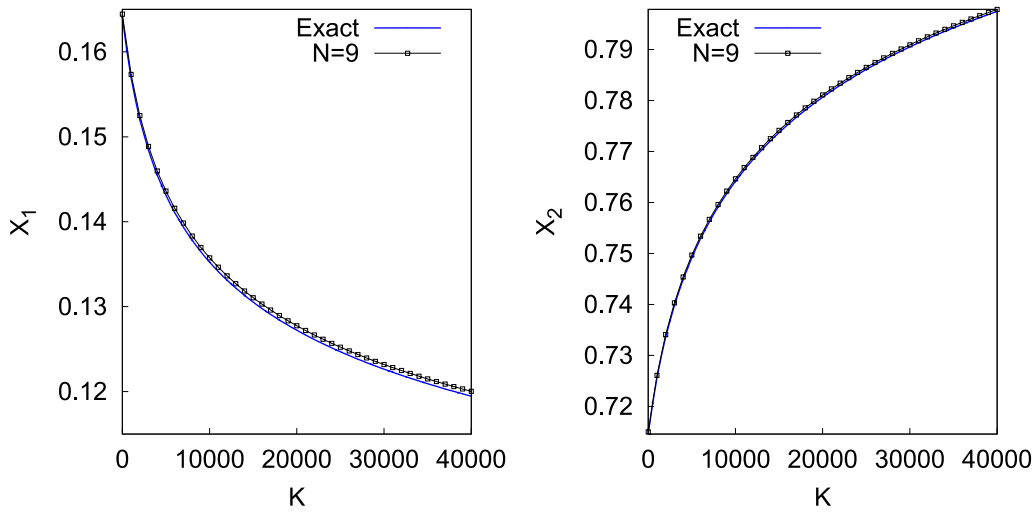

Fig. 10 Case (3) parametric study for exact solution and RRM

Table 10 Integration constants for exact solutions of cases (4)

	***Region*(1)** $x \in [0, 0.104030928]$	***Region*(2)** $x \in [0.104030928, 0.3]$	***Region*(3)** $x \in [0.3, 0.7]$	***Region*(4)** $x \in [0.7, 0.895969072]$	***Region*(5)** $x \in [0.895969072, 1]$
C_1	0	$-6.798279134 \times 10^{-5}$	-0.00554338148	-0.0019940451	0
C_2	0	$2.466183884 \times 10^{-5}$	0.01712644656	$3.216033831 \times 10^{-4}$	0
C_3	0	$1.028271896 \times 10^{-5}$	$-1.831498818 \times 10^{-4}$	$1.718982154 \times 10^{-7}$	0
C_4	0	$-2.834532907 \times 10^{-5}$	$-1.966540429 \times 10^{-4}$	$-1.06582459 \times 10^{-6}$	0
A	0	0	9375/32	0	0
B	0	0	$-9375/16$	0	0
C	0	0	26625/64	0	0
D	0	0	$-7875/64$	0	0
E	0	0	6615/512	0	0
F	0	0	0	0	0
G	0	0	0	0	0
H	$5.55320932 \times 10^{-4}$	0	0	0	$-5.55320932 \times 10^{-4}$
I	$-5.77705521 \times 10^{-5}$	0	0	0	$4.975503799 \times 10^{-4}$

3.4.3 Parametric study

The variation of x_1 and x_2 against stiffness is shown in Fig. 13A and B, respectively. As $\overline{K}$ increases, the value of the first lift-off point, x_1, increases. And the value of the second lift-off point, x_2, decreases. Hence, the contact length decreases as $\overline{K}$ and the soil resistance increases. In this case, also, RRM accuracy is illustrated by comparison with the exact solution (Table 12).

3.5 Case (5)

So far, the accuracy of the Rayleigh–Ritz procedure was illustrated for beams with constant inertia, i.e., $i(x) = 1$. Generally, exact solutions cannot be obtained for the case of a beam of variable inertia, i.e., $i(x) \neq$ constant. Hence, this is a typical case to further illustrate the power of the proposed method because only RRM solutions can be presented.

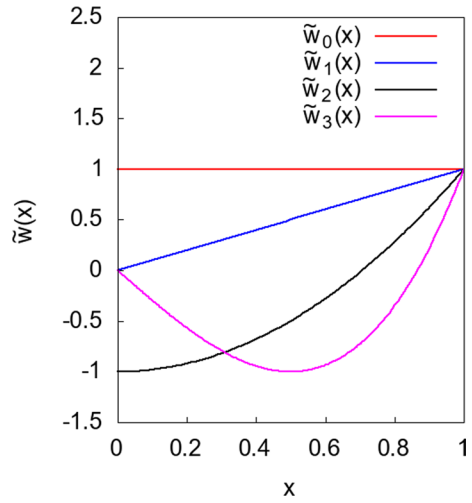

Fig. 11 Mode shapes for a beam with free ends

Table 11 Lift-off points x_1 and x_2 at $q = q_4$ for various N The exact value $x_1 = 0.104030928$ and $x_2 = 0.895969072$

N	x_1	x_2
7	0.112583071	0.8942908347
8	0.1158445179	0.8972961009
9	0.1048439443	0.8945482671
10	0.1045830548	0.8946845233
11	0.1041499674	0.8960036337
12	0.1042748392	0.8960353434
13	0.104013592	0.8960037529
14	0.1038406193	0.8959776461
15	0.1040145457	0.89597103

For a beam with free ends, consider the load $q = q_5$ is defined as in Eq. (46) and the variable beam inertia is defined as:

$$i(x) = 1 + x(1 - x) \tag{51}$$

3.5.1 RRM solution

Similar to the previous case, the same shape function and procedure are followed to get the beam deflection. Starting with an initial guess of $x_1 = 0.1$ and $x_2 = 0.9$. The converged values of x_1 and x_2 for different N are provided in Table 13. For $N = 13$ and $N = 15$ values, convergence is achieved in 4 and 5 iterations, respectively.

Since there is not an available exact solution, the RRM solution at a rather high-order $N = 15$ will be used as a reference to calculate errors defined as $100 \times (\widetilde{w}_{N=15} - \widetilde{w}_N)/\max\left|\widetilde{w}_{N=15}\right|$.

From Eq. (15) and using the coefficients of RRM solutions provided in Table 14, $\widetilde{w}_{N=15,\max} = \widetilde{w}_{N=15}(x = 0.4999596775) = 1.61531522 \times 10^{-4}$. The lift-off points for $N = 15$ are determined as $x_1 = 0.084852844$ and $x_2 = 0.915140122$.

Results are shown for RRM solutions at orders $N = 7, 11, 13, 15$ in Fig. 14A. The percentage error in deflection of $N = 11$ compared to $N = 15$ is less than or equal to 0.24%, and for $N = 13$ the percentage error in deflection shown in Fig. 14B is negligible. The convergence of RRM shear and moment toward the exact values is illustrated in Fig. 14C and D, respectively.

3.5.2 Parametric study

The variation of $x_1$andx_2 against stiffness is shown in Fig. 15A and B, respectively. Similar to case (4), the value of the first lift-off point, x_1, increases, and the value of the second lift-off point, x_2, decreases. Hence, the contact length decreases as $\overline{K}$ and the soil resistance increases. In this case, also, RRM accuracy is illustrated by comparison with the exact solution.

4 Conclusions

Approximate, yet accurate analytical detailed solutions for the problem of a beam resting on tensionless soil are presented. The Rayleigh–Ritz procedure is implemented using MAXIMA symbolic package. An iterative procedure is developed to model the nonlinear stiffness along with the identification of lift-off points. The iterative method converges within a few trials. The compatibility conditions are satisfied automatically simply and straightforwardly within the developed iterative method.

The exact solutions are presented and derived for relatively simple cases. The accuracy of the iterative Rayleigh–Ritz method is illustrated through comparison with exact solutions. The method's success is illustrated by clamped and free-end supports. For each case, the shape functions used for the Rayleigh–Ritz method are provided. Convergence toward the exact results is illustrated as the order of the Rayleigh–Ritz method is increased.

Finally, the power of the Rayleigh–Ritz method is illustrated by modeling a beam with variable inertia. The significance of this problem is high since obtaining an exact solution is very difficult. The accuracy of the method is

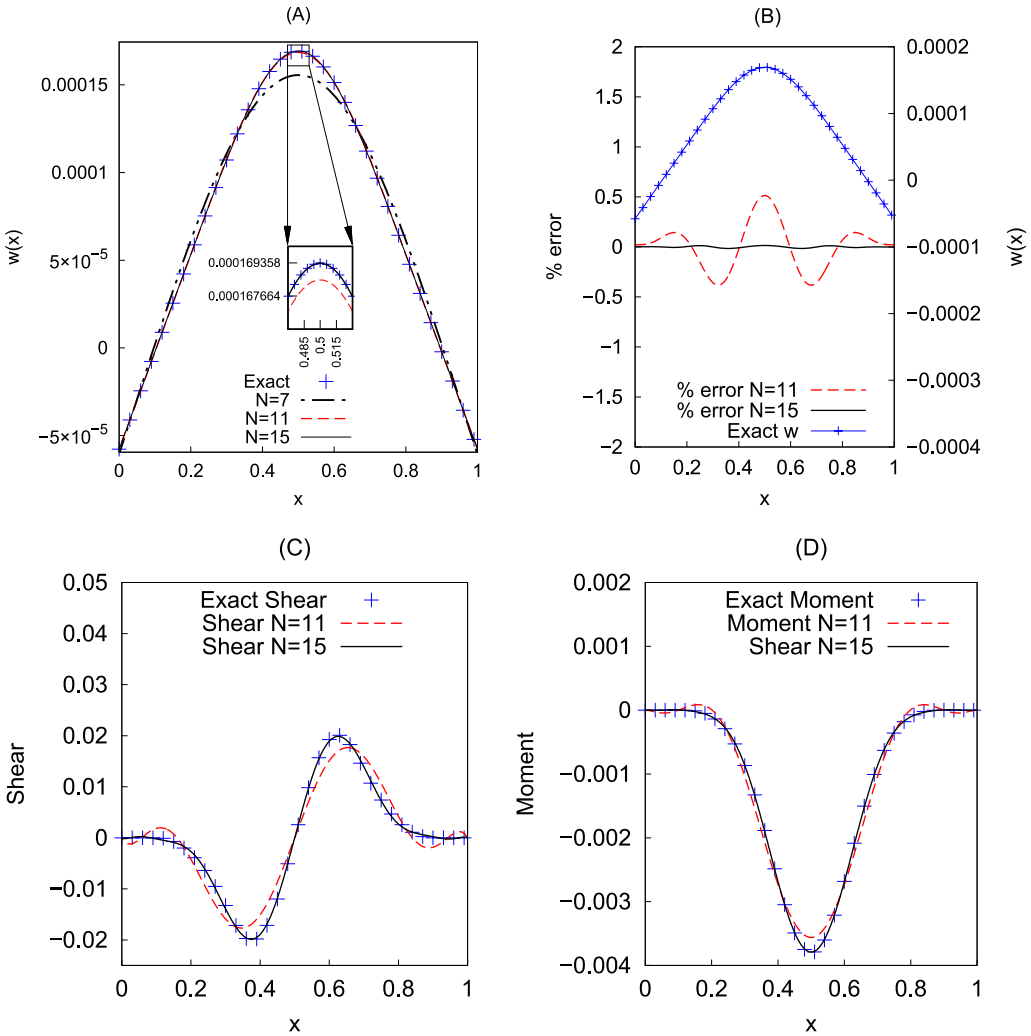

Fig. 12 Case (4) RRM and exact results. **A** Exact solution and RRM deflection. **B** Exact deflection and percentage error for various orders. **C** Exact and RRM shear. **D** Exact and RRM moment

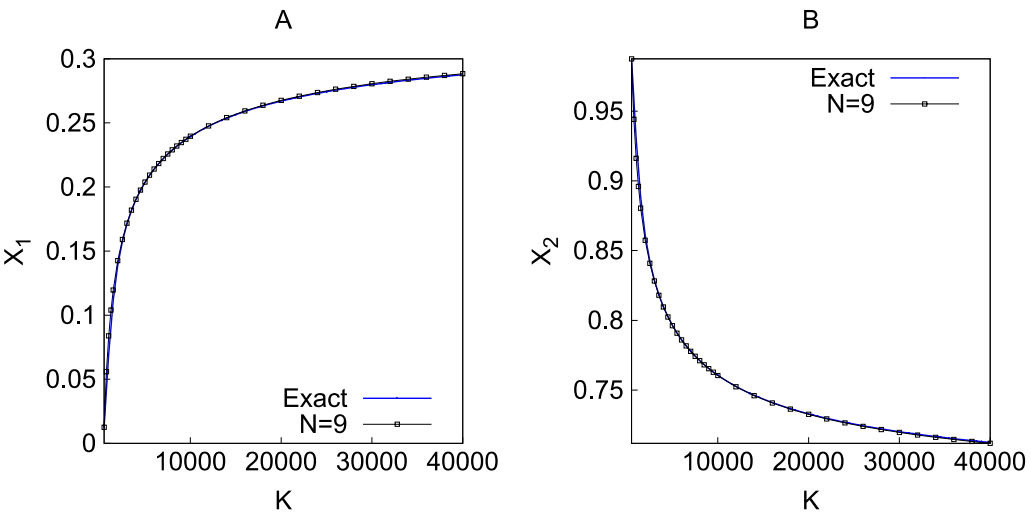

Fig. 13 Case (4) Parametric Study for Exact Solution and RRM. **A** Variation of x_1 with the soil stiffness (K). **B** Variation of x_2 with the soil stiffness (K)

Table 12 Coefficients a_i for various N of Rayleigh–Ritz procedure in case (4)

Coefficients a_i	$N = 15$	$N = 11$	$N = 9$
a_1	−12.11644098	−0.2443290684	0.02564239328
a_2	23.16072979	0.4598013053	−0.04768563563
a_3	−20.20919553	−0.3823959623	0.03834732574
a_4	16.07137737	0.2798265612	−0.02646196004
a_5	−11.61393415	−0.1789399189	0.01520990135
a_6	7.592365735	0.09856403472	−0.007169912679
a_7	−4.461734475	−0.0457998286	0.002646214949
a_8	2.336536222	0.01738868058	$-6.705508312 \times 10^{-4}$
a_9	−1.077289308	−0.005086442519	$8.407102566 \times 10^{-5}$
a_{10}	0.4299316184	0.001014930822	–
a_{11}	−0.1448997899	$-1.020244299 \times 10^{-4}$	–
a_{12}	0.03971007583	–	–
a_{13}	−0.008307533284	–	–
a_{14}	0.001177597947	–	–
a_{15}	$-8.441222046 \times 10^{-5}$	–	–

Table 13 Lift-off points x_1 and x_2 at $q = q_5$ for various N

N	x_1	x_2
7	0.094434828	0.912301093
8	0.096135348	0.915150970
9	0.085173637	0.914209634
10	0.084836632	0.914269417
11	0.084785730	0.915231556
12	0.084908932	0.915254384
13	0.084834427	0.915165752
14	0.084763974	0.915150374
15	0.084852844	0.915140122

verified by comparing the results of various orders with that of a very high order.

The method is further applied to conduct parametric studies and gain more insight into the problem of physics. The contact length inverse proportionality to the soil stiffness is presented for all cases. Hence, the influence of soil stiffness on the beam–soil interaction is illustrated.

The accuracy and efficiency of the method are illustrated. The results may be used in the future to verify numerical results. Also, the method may be extended for Pasternak soil types. In addition, tensionless cubic soil resistance deflection relationships can be modeled.

Table 14 Coefficients a_i for various N of Rayleigh–Ritz procedures in case (5)

Coefficients a_i	$N = 15$	$N = 13$	$N = 11$
a_1	−9.621729056	1.26509266	−0.1934752187
a_2	18.39089276	−2.402425146	0.3641356857
a_3	−16.04410765	2.054943739	−0.3028682506
a_4	12.75497774	−1.579207895	0.2216699238
a_5	−9.213226612	1.085004054	−0.1418129818
a_6	6.01949861	−0.6617807486	0.0781559243
a_7	−3.534956678	0.3545439777	0.03633997966
a_8	1.849693568	−0.1642435165	0.01380962478
a_9	−0.8520413131	0.06429408045	−0.004043946098
a_{10}	0.3396967581	$-0.020516978 \times 10^{-2}$	$8.075018814 \times 10^{-4}$
a_{11}	−0.1143678132	$0.005015763 \times 10^{-3}$	$-8.115198537 \times 10^{-5}$
a_{12}	0.03131058729	$-8.326536226 \times 10^{-4}$	–
a_{13}	−0.006544519907	6.9774709×10^{-5}	–
a_{14}	$9.271890423 \times 10^{-3}$	–	–
a_{15}	$-6.647133278 \times 10^{-5}$	–	–

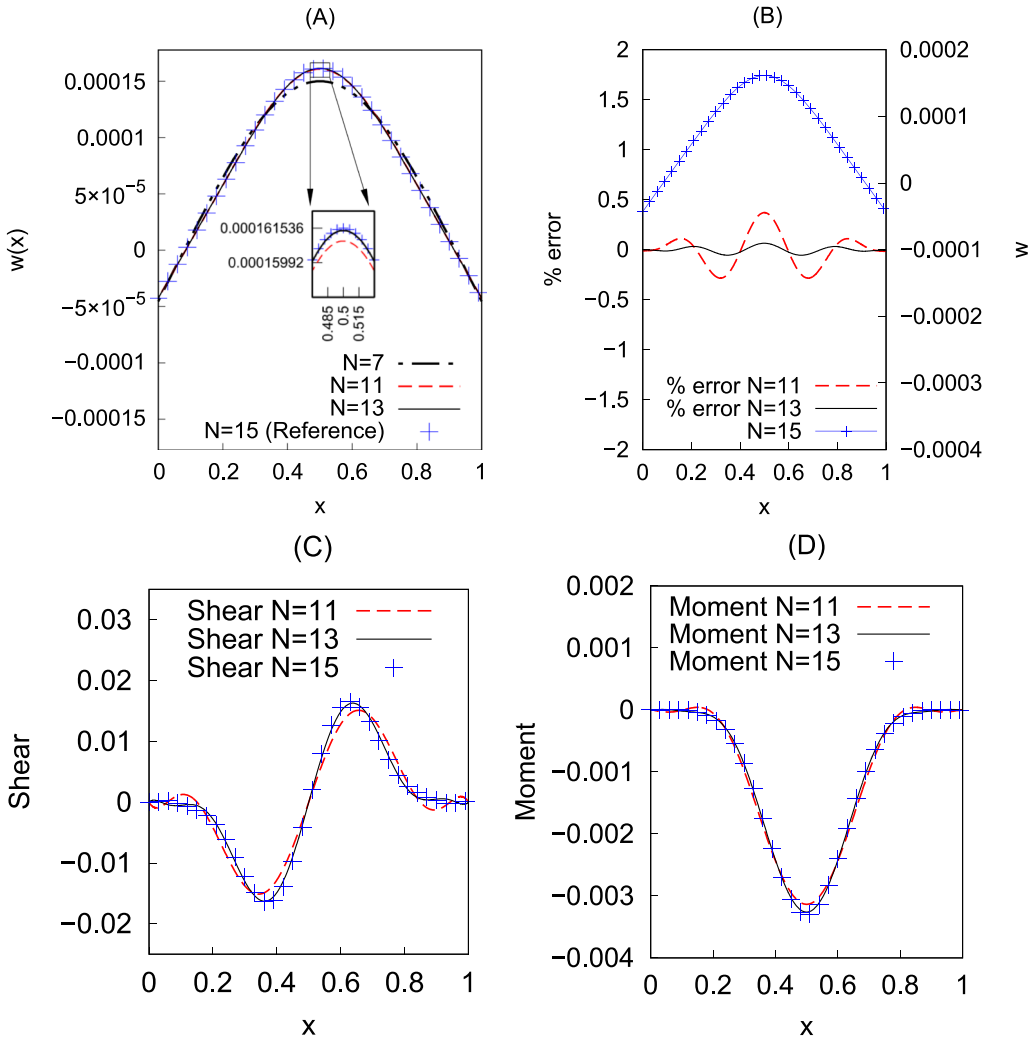

Fig. 14 Case (5) RRM and exact results. **A** Exact solution and RRM solutions. **B** Exact deflection and percentage error for various orders. **C** Exact and RRM shear. **D** Exact and RRM moment

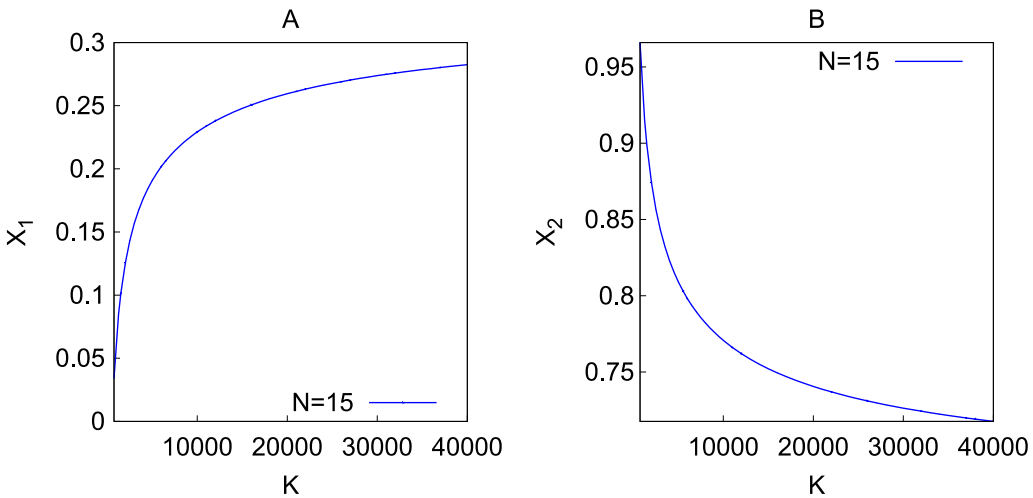

Fig. 15 Case (5) Parametric Study for Exact Solution and RRM. **A** Variation of x_1 with the soil stiffness (K). **B** Variation of x_2 with the soil stiffness (K)

Abbreviation
RRM: Raleigh–Ritz method.

Acknowledgements
Not applicable.

Author contributions
TH team leader who initiated the concept of the current paper and derived the governing equations. HA performed the analytical solution and parametric study for different cases. ME conducted the discussion of results reviewed the manuscript. All authors have read and approved the manuscript.

Funding
Not applicable.

Availability of data and material
Not applicable.

Declarations

Ethics approval and consent to participate
Not applicable.

Consent for publication
Not applicable.

Competing interests
The authors declare that they have no competing interests.

Author details
[1]Mechanical Power Engineering Department, Faculty of Engineering, Cairo University, Giza 12613, Egypt. [2]Department of Engineering Mathematics and Physics, Faculty of Engineering, Cairo University, Giza, Egypt. [3]Smart Engineering Systems Center (SESC), Nile University, Shaikh Zayed, Giza, Egypt.

Received: 27 July 2022 Accepted: 6 December 2022
Published online: 23 December 2022

References

1. Javaid O, Choi DH (2020) Effect of track irregularities on the response of two-way railway tracks. Appl Sci 10(1):11. https://doi.org/10.3390/app10010011
2. Zhang L, Zhao M (2015) New method for a beam resting on a tensionless and elastic-plastic foundation subjected to arbitrarily complex loads. Int J Geomech 16(4):04015093. https://doi.org/10.1061/(ASCE)GM.1943-5622.0000577
3. Zhang Y, Murphy KD (2004) Response of a finite beam in contact with a tensionless foundation under symmetric and asymmetric loading. Int J Solids Struct 41(24–25):6745–6758. https://doi.org/10.1016/J.IJSOLSTR.2004.05.028
4. Bhattiprolu U, Bajaj AK, Davies P (2013) An efficient solution methodology to study the response of a beam on viscoelastic and nonlinear unilateral foundation: Static response. Int J Solids Struct 50(14–15):2328–2339. https://doi.org/10.1016/J.IJSOLSTR.2013.03.014
5. Zhang Y, Liu X (2019) Response of an infinite beam resting on the tensionless Winkler foundation subjected to an axial and a transverse concentrated load. Eur J Mech A Solids 77:103819. https://doi.org/10.1016/J.EUROMECHSOL.2019.103819
6. Bhatra S, Maheshwari P (2019) Double beam model for reinforced tensionless foundations under moving loads. KSCE J Civ Eng 23(4):1600–1609. https://doi.org/10.1007/s12205-019-1609-6
7. Dimitrovová Z (2017) New semi-analytical solution for a uniformly moving mass on a beam on a two-parameter visco-elastic foundation. Int J Mech Sci 127:142–162
8. Zhang L, Zhao M (2016) New Method for a Beam Resting on a Tensionless and Elastic-Plastic Foundation Subjected to Arbitrarily Complex Loads. Int J Geomech 16(4):04015093. https://doi.org/10.1061/(ASCE)GM.1943-5622.0000577
9. Güler K (2004) Circular elastic plate resting on tensionless Pasternak foundation. J Eng Mech 130(10):1251–1254. https://doi.org/10.1061/(ASCE)0733-9399(2004)130:10(1251)
10. Abbas W, Bakr OK, Nassar MM, Abdeen MAM, Shabrawy M (2021) Analysis of tapered Timoshenko and Euler-Bernoulli beams on an elastic foundation with moving loads. J Math. https://doi.org/10.1155/2021/6616707
11. Elshabrawy M, Abdeen MA, Beshir S (2021) Analytic and numeric analysis for deformation of non-prismatic beams resting on elastic foundations. Beni Suef Univ J Basic Appl Sci 10(1):1–11. https://doi.org/10.1186/S43088-021-00144-5/FIGURES/4
12. Holmes MH (2009) Introduction to the foundations of applied mathematics, vol 56. Springer, New York. https://doi.org/10.1007/978-0-387-87765-5
13. Heshmat T, Elshabrawy M (2021) Analytical solution for nonlinear interaction of Euler beam resting on a tensionless soil. In: Proceedings of international structural engineering and construction, 2021, vol 8, no. 1, pp GFE-021–GFE-02-6. https://doi.org/10.14455/ISEC.2021.8(1).GFE-02
14. Gelagoti F, Georgiou I, Kourkoulis R, Gazetas G (2018) Nonlinear lateral stiffness and bearing capacity of suction caissons for offshore wind-turbines. Ocean Eng 170:445–465. https://doi.org/10.1016/j.oceaneng.2018.10.020
15. Das AK, Deb K (2017) Response of cylindrical storage tank foundation resting on tensionless stone column-improved soil. Int J Geomech 17(1):04016035. https://doi.org/10.1061/(ASCE)gm.1943-5622.0000697
16. Farid AF, Rashed YF (2018) BEM for thick plates on unilateral Winkler springs. Innov Infrastruct Solut. https://doi.org/10.1007/s41062-018-0128-5
17. Payette GS, Reddy JN (2010) Nonlinear quasi-static finite element formulations for viscoelastic Euler–Bernoulli and Timoshenko beams. Int J Numer Method Biomed Eng 26(12):1736–1755. https://doi.org/10.1002/CNM.1262
18. Hsu YS (2020) Finite element approach of the buried pipeline on tensionless foundation under random ground excitation. Math Comput Simul 169:149–165. https://doi.org/10.1016/J.MATCOM.2019.09.004
19. Wang Y, Qiao P, Lu L (2018) Buckling analysis of steel jacking pipes embedded in elastic tensionless foundation based on spline finite strip method. Thin-Walled Struct 130:449–457. https://doi.org/10.1016/j.tws.2018.06.010
20. Beghami W, Maayah B, Bushnaq S, Abu Arqub O (2022) The Laplace optimized decomposition method for solving systems of partial differential equations of fractional order. Int J Appl Comput Math 8(2):1–18. https://doi.org/10.1007/S40819-022-01256-X/FIGURES/6
21. Olver PJ (1986) Applications of Lie groups to differential equations, vol 107. Springer, New York. https://doi.org/10.1007/978-1-4684-0274-2
22. Arqub OA, Hayat T, Alhodaly M (2022) Analysis of Lie symmetry, explicit series solutions, and conservation laws for the nonlinear time-fractional phi-four equation in two-dimensional space. Int J Appl Comput Math 8(3):1–17. https://doi.org/10.1007/S40819-022-01334-0
23. Abu Arqub O (2018) Numerical solutions for the Robin time-fractional partial differential equations of heat and fluid flows based on the reproducing kernel algorithm. Int J Numer Methods Heat Fluid Flow 28(4):828–856. https://doi.org/10.1108/HFF-07-2016-0278/REFERENCES
24. Abu Arqub O (2015) Reproducing kernel algorithm for the analytical-numerical solutions of nonlinear systems of singular periodic boundary value problems. Math Probl Eng. https://doi.org/10.1155/2015/518406
25. Cassel KW (2013) Variational methods with applications in science and engineering. Var Methods Appl Sci Eng 9781107022584:1–413. https://doi.org/10.1017/CBO9781139136860
26. Mason JC, Handscomb DC (2002) Chebyshev polynomials. Chapman and Hall/CRC, Boca Raton. https://doi.org/10.1201/9781420036114

Publisher's Note